1995

Shape optimization of Navier-Stokes flows with application to optimal design of artificial heart components

Omar Ghattas
Carnegie Mellon University

Beichang He

James F. Antaki

Carnegie Mellon University.Engineering Design Research Center.

Shape Optimization of Navier-Stokes Flows with Application to Optimal Design of Artificial Heart Components

Omar Ghattas, Beichang He, James F. Antaki

EDRC 12-67-95

SHAPE OPTIMIZATION OF NAVIER-STOKES FLOWS WITH APPLICATION TO OPTIMAL DESIGN OF ARTIFICIAL HEART COMPONENTS [1]

Omar Ghattas **Beichang He**
Computational Mechanics Laboratory
Department of Civil and Environmental Engineering
Carnegie Mellon University
Pittsburgh, PA 15213
{oghattas,**bhe}@cs.emu.edu**

James F. Antaki
Artificial Heart Program
Department of Surgery
University of Pittsburgh Medical Center
Pittsburgh, PA 15213
antakiQpitt**surg**.nb•**upmc**.**edu**

Abstract

We consider the problem of shape optimization of systems governed by the stationary incompressible Navier-Stokes equations under flow and geometric constraints. Our motivation stems from the problem of optimal design of artificial heart components. An continuation-SQP algorithm is developed to efficiently couple Newton-based optimization and flow solution. The main feature of the algorithm is to decompose the optimization problem into a sequence of subproblems characterized by increasing Reynolds numbers, and then apply continuation schemes on the design field, Hessian matrix, Lagrange multipliers, and flowfield. As an application we consider the optimum design of the shape of a two dimensional tube—a simplification of a blood flow cannula that is a component of an artificial heart. Representative numerical results show a factor of four improvement in efficiency over a standard SQP algorithm.

1. Introduction

The shape optimization problem is to minimize or maximize, through variation of a domain boundary or portion thereof, an objective function, subject to constraints imposed by a boundary value problem as well as other physical and geometrical conditions. It arises in a variety of engineering applications. An example is the optimum design of systems governed by viscous, incompressible flows. Conventional trial-and-error design methods often prove to be time-consuming, expensive, and ineffective in addressing such design problems. Advances in computational fluid dynamics (CFD), numerical optimization methods, and high performance computing have made it possible for us to envision computer-based systems that will automate the design of such systems. The challenges to the development of such systems are manifold:

[1] **This work is supported by the Engineering Design Research Center, an NSF Engineering Research Center at Carnegie Mellon University.**

- design variables that effectively parameterize complex geometries must be identified,
- appropriate objective functions and constraints must be derived to account for the desired functionality,
- efficient numerical methods for optimization, flow simulation, and their coupling must be developed, and
- these methods must be translated into parallel algorithms and mapped onto high performance computers.

Most of the existing literature relevant to shape optimization of fluid flows is in the context of aerodynamics [1] [3] [4] [11] [13] [14] [16]. Aerospace and aeronautical engineering often deal with high Reynolds number flows, where viscous effects are typically important only within a thin layer near the boundary. Thus viscosity is ignored in most aerodynamic shape optimization work, and fluid flow is modeled with the full potential or Euler equations. Recent work has included the viscous effects with the thin-layer Navier-Stokes equations [5]. However, there are many applications in which an inviscid assumption is not warranted, and the full Navier-Stokes equations have to be used. Some published work exists in this direction. Pironneau derives first-order optimality conditions for the minimum-drag problem [15]. Numerical solution of the nonlinear algebraic equations derived from these first-order conditions is later attempted, but a number of approximations are introduced due to the limited computing power of the 1970s [8]. Another application and extension of this work is [2], where the optimum profile of a channel or duct is sought based on continuum sensitivity analysis and a simple optimization algorithm.

In this study we consider the problem of shape optimization of systems governed by the stationary incompressible Navier-Stokes equations under flow and geometry constraints. Our interest in this work is motivated by the desire to optimize the design of an artificial heart device, specifically a complete blood pump and its connecting conduits. Due to the difficulty of solving a large nonlinear optimization problem and parameterizing the complex geometry, we first concentrate on a problem that has been simplified with respect to geometry and dimensionality. In this paper we discuss shape optimization of a two dimensional tube representing the inflow cannula of a circulatory assist device. Several different objective functions are proposed to indirectly and directly model blood damage. Despite the simplifications made, this problem retains many of the features and the same mathematical structure as the general problem, thus allowing us to develop insight into solution properties, sensitivity of the optimum to various problem data, influence of different objective functions, performance of algorithms, etc. Furthermore, the design of an artificial heart cannula has proven to be a challenge in the past due to the complex flow characteristics and the sparse theoretical and experimental results available.

We discretize the Navier-Stokes equations by Galerkin finite elements; the resulting system of nonlinear algebraic equations is solved by a Newton-continuation method. First order design sensitivities are computed analytically after discretization. The nonlinearly-constrained optimization problem is solved by a sequential quadratic programming (SQP) method that requires only gradients of the objective and constraints. A continuation-SQP algorithm is introduced to improve convergence and efficiency of the optimization process. The main feature of this algorithm is to decompose the optimization problem into a sequence of subproblems characterized by increasing Reynolds numbers. Continuation schemes on the

design field, Lagrangian Hessian matrix, Lagrange multipliers, and flowfield are then applied. Several problems of finding the optimal shape of a two dimensional tube to minimize a model of blood damage are solved.

The rest of the paper is organized as follows. Section 2 establishes the governing flow equations and objective functions of interest, and formulates the shape optimization problem. Section 3 reviews discrete sensitivity analysis and optimization of nonlinear systems. Section 4 introduces an efficient algorithm to couple the SQP optimizer and the flow solver through a continuation scheme. Section 5 specializes the optimization method to the problem of optimal design of a two dimensional tube, and Section 6 presents some representative numerical results. We conclude with some remarks in Section 7.

2. Mathematical Formulation

Stationary, incompressible, Newtonian fluid flow in a domain *Q,* is governed by the Navier-Stokes equations, i.e. the conservation of momentum equation

$$p(v\text{-}V)v\text{-}V.cr = g, \tag{1}$$

the constitutive law

$$\boldsymbol{\sigma} = -p\mathbf{I} + \mu(\nabla\mathbf{v} + \nabla\mathbf{v}^T), \tag{2}$$

and the conservation of mass equation

$$V.v = 0, \tag{3}$$

where v is the fluid velocity, *a* the stress tensor, p the pressure, g the body force, *p* the fluid density, and /i the dynamic viscosity. A Newtonian constitutive law is the simplest model of blood, with \i taken to be an approximate asymptotic value (4.0 cps).

The following local and global functions are proposed to model blood damage; they are relevant to other applications as well. They may be introduced as objective or constraint functions.

- The rate of energy dissipation due to viscosity:

$$\$ = \underline{lp}(Vv + Vv^r) : (Vv + Vv^T) \tag{4}$$

- Maximum shear stress, e.g. in two dimensions:

$$\mathbf{r}_{\mathbf{m}}{}^{*}_{\underline{x}} = \sqrt{11\left(\frac{\sigma_{xx}}{2}\right)\mathbf{J} + o|_y} \tag{5}$$

- Magnitude of vorticity:

$$u> = |V \times v| \tag{6}$$

- Integral of the dissipation function over flow domain, both unsealed and scaled by area or volume of the domain:

$$Jn^{\Phi\, d\Omega}, \qquad \hat{\Phi} = \frac{\overline{\Phi}}{\int_\Omega d\Omega} \tag{7}$$

- **Integral of maximum shear stress, both unsealed and scaled:**

$$\bar{\tau} \text{ -L } Tmaxdil, \qquad f = \frac{\bar{\tau}}{\int_\Omega d\Omega} \tag{8}$$

- **Integral of vorticity magnitude, both unsealed and scaled:**

$$\overline{LJ} = \int^{t} u \, dQ,, \qquad Q = \frac{\bar{\omega}}{\text{-}\,\omega} \tag{9}$$

The critical micro flow criteria for the design of artificial heart components are (1) minimizing blood damage (hemolysis) and (2) avoiding blood clotting (thrombosis). It is well known that blood damage is directly related to high shear stresses and exposure times experienced by blood cells. In addition, the existence of regions of recirculation and stagnation have been demonstrated to bear strong correlation to the onset of clotting and to the deposition of blood elements within prosthetic devices. The above functions involving vorticity and dissipation are reasonable mechanisms for reducing recirculation and thus thrombosis, while the shear stress functions are directly related to hemolysis of blood.

We may choose any convex combination of the six global functions in Equations (7)-(9) as our objective function. In addition, limits on allowable values of the local functions (4)-(6) may be introduced as inequality constraints. Conditions which ensure a valid shape and limit the size of the shape have to be introduced as geometric constraints. We will discuss such geometric constraints in Section 5 in the context of a two dimensional tube. An appropriate statement of a continuous problem arising in the optimum design of an artificial heart device might be, for example, to minimize the integral of dissipation $\bar{\$}$ in (7), subject to geometry and physics constraints, including equalities in the form of the Navier-Stokes equations (1), (2), and (3), and inequalities induced by demanding that the local maximum shear stress (5) not exceed an allowable value throughout the domain. The aspect of the design that we have under our control is its boundary (or part of it). Thus, this problem is one of shape optimization.

3. Numerical Optimization

The shape optimization problem described in the previous section cannot be solved in closed form; thus, we seek a numerical solution. By discretizing the flow domain and approximating the field variables with finite elements, the discrete form of the governing flow equations as well as the global functions (7)-(9) can be expressed as the sum of integrals over each element. On the other hand, the local functions (4)-(6) are defined pointwise; thus, it is appropriate to define them at element centroids. A finite number of design variables results from a suitable parameterization of the shape. The resulting optimization problem can then be stated as finding, from the space of shapes spanned by the shape parameterization, the one that minimizes the objective while satisfying the constraints. The problem can thus be transformed into a nonlinear programming problem (NLP).

The approach taken to solve the NLP is to eliminate the governing state equations (the discrete Navier-Stokes equations) and state variables (velocities and pressures) at each design iteration by solving them for the current shape. The values of the state variables are then

used to evaluate the objective function. The implicit function theorem is invoked to find gradients of objective and constraint functions. In the future we will consider methods that retain the state equations as equality constraints, thereby obviating the need for flow solution at each iteration [14]. An SQP method is used to solve the optimization problem. It makes use of a quasi-Newton, in particular a BFGS, approximation to the reduced Hessian; thus, only first derivatives of the objective and constraints with respect to design variables are required.

We begin with the weak form of the Navier Stokes equations,

Find v € H^1 (ft) and p € L^2 (ft) such that:

$$a(v, w) + 6(p, w) + c(v, v, w) = 0 \qquad \text{for all } w \in H^1(ft), \tag{10}$$

$$\&(g,v) = 0 \qquad \text{for all } q \in L^2(ft),$$

where

$$a(v, w) = \int_{\Omega} | (Vv + Vv^T) : (Vw + Vw^T) \; dft, \tag{11}$$

$$\&(p,w) = - \int_{Jn} pV \cdot w \, dft, \tag{12}$$

and

$$c(v,v,w) = \int_{Jn} pw(v > V)v \, dft. \tag{13}$$

Here, H^1 (ft) is the Sobolev subspace of all functions having one square integrable derivative over ft and that satisfy the homogeneous essential boundary conditions, and L^2 (ft) is the space of functions that are square integrable over ft.

Upon introduction of the finite element approximations v^ and *ph*, i.e.

$$\mathbf{v}_h = \sum_{i=1}^{n^v} \phi_i(\mathbf{x}) v_i, \qquad p_h = \sum_{i=1}^{n^p} \chi_j(\mathbf{x}) p_j, \tag{14}$$

we obtain the discrete problem corresponding to Galerkin's method,

Find Vfc £ *Vh* and *ph* 6 *Vh* such that

$$a(vji, w_{fc}) + 6(p/_l, w_{fc}) + c(v^\wedge, v_{fci}\, w_{fc}) = 0 \qquad \text{for all } w^\wedge \in V^*, \tag{15}$$

and

$$b\{q,v_h) = 0 \qquad \text{for all } q \in V_h,$$

where the finite element spaces *Vh* and *Vh* for velocity and pressure,

$$V_h = \text{span}\{<£!,...,</>_{„*}\}, \qquad Pfc = \text{span}\{xi,...,Xnp\}, \tag{16}$$

are subspaces of the infinite dimensional spaces in (10), i.e. *Vh* C H^x(ft) and *Vh* C $L^2(Q)$. The discrete problem (15) is a set of nonlinear coupled algebraic equations, consisting of the n^v discrete conservation of momentum equations,

$$\sum_{t=l}^{n^v} '£_i a(<l>_i,4>t)vi + \sum_{j=l}^{nP} '52Kxj,<l>t)Pj + \sum_{t,r=l}^{n^v} E\, c(<f>_h<t>_r,(j>_e)viV_r = 0 \qquad ^\wedge = 1,\ldots,n^v, \tag{17}$$

and the n^p discrete conservation of mass equations,

$$\sum_{i=1}^{n^v} b(\backslash m,<fc>.- = 0 \qquad m = l,\ldots,7i». \tag{18}$$

See, for example, [9] for details on finite element approximation of Navier-Stokes flows.

Let us represent the discrete momentum equations (17) as $h_v = 0$ and the discrete mass equations (18) as $h_p = 0$, and let us define vectors of unknown nodal quantities by letting v 6 9ft^{nV} represent the fluid nodal velocities and p 6 5f^{nP} the fluid nodal pressures. We refer to the combined vector u where,

$$\mathbf{u}^T = \left(\mathbf{v}^T, \mathbf{p}^T\right)$$

as the state variable vector, and its elements as the state variables, and the combined equations h = 0 where

$$\mathbf{h}^T = \left(\mathbf{h}_v^T, \mathbf{h}_p^T\right),$$

as the state equations, and h as the state equation residual.

Next we outline the computation of gradients of the objective and constraints with respect to design variables, i.e. the design sensitivity analysis problem. Here, we have chosen to discretize first, and then differentiate, as opposed to the reverse. Certainly, the reverse is possible, e.g. [15], and under certain conditions the two approaches yield identical gradients.

Symbolically, if the design variables are represented by TT, the discrete form of any of the scalar functions of (4)-(9) can be written in the general form

$$« = ¥(u(ir),ir), \tag{19}$$

where the dependence of $ on TT is both implicit through the dependence of u on TT, as well as explicit. Thus, the gradient of $ with respect to the design variables TT is given by

$$\frac{D\Psi}{DlZ} \sim \overline{8W} \wedge \overline{dTT}\ \overline{On'} \tag{20}$$

The Jacobian of the state variables u with respect to the design variables TT can be found by differentiating the state equations h(u(?r), TT) = 0 with respect to TT and solving the resulting system

$$*\mathbf{L}\,*\mathbf{i} = -*\mathbf{L} \tag{21}$$

for *du/dir*. Using the chain rule and the above results, and representing the Jacobian of h with respect to u as the matrix J, we obtain

$$\frac{D\Psi}{Dw} \sim 8^* \underline{dx}^T \underline{dv} - \underline{dx}^T \underline{dh}^T \mathbf{r} \leq \underline{w} \tag{22}$$

where x represents the mesh coordinates. Depending on whether the product

$$\mathbf{J}^{-1}\frac{\partial \mathbf{h}}{\partial \pi} \quad \text{ш} \quad \mathbf{J}^{-T}\frac{\partial \Psi}{\partial \mathbf{u}}$$

is formed first, the sensitivity analysis method is known as either *direct* or *adjoint*[1].

[1] **Of course, J is not inverted; is solved for the appropriate righthand side vector.**

The Jacobian of x with respect to TT is known as the *design velocity field,* and depends on the mesh generation process. For general geometries and meshes, the design velocity field may be computed by an elastic analogy.[2] However, here we optimize geometries that are meshable in closed form, and thus we compute the design velocity field analytically.

4. Continuation-SQP algorithm

SQP is generally regarded as the most efficient general method for solution of nonlinearly-constrained smooth optimization problems [12]. It can be viewed as a Newton method for solving the first order optimality conditions of the nonlinear optimization problem (e.g. [7]). It works by solving a sequence of linearly-constrained quadratic optimization problems, in which the objective is a quadratic approximation of the Lagrangian function, and the constraints are linear approximations of the nonlinear constraint set. In this work, a quasi-Newton approximation is used for the Hessian matrix of the Lagrangian function, thereby avoiding the need to compute second derivative information. For the purposes of this **paper,** we simply think of each iteration of SQP as a procedure for advancing values of the design variables, given values of the objective functions and its gradient, and the constraint functions and their Jacobian matrix. The design variables are updated in this manner until an optimum is reached.

The most straightforward SQP algorithm for solving the discretized Navier-Stokes shape optimization problem couples the optimizer and flow solver in such a way that the former drives the latter by feeding it with shape parameters, while the latter serves the former by providing it with values of the objective function and constraints, and their design sensitivities. Thus, Algorithm 1 shown in Figure 1 results. For clarity of presentation, we restrict ourselves to the case in which constraints only consist of discrete state equations. The objective is denoted by \P. A simple Newton-continuation method is used to globalize the flow solver: the flow is converged for a low Reynolds number problem; the Reynolds number is increased; the flow solver is initiated with the solution from the previous Reynolds number problem; and the loop is repeated until the target Reynolds number is reached. We refer to this algorithm as a "black-box" method, in the sense that flow solver and optimizer are completely distinct, and they couple in the least possible way during optimization. For each shape, the flow is solved fully for the target Reynolds number. We use the term "black-box" despite the fact that analytical gradients are used, in order to contrast this approach with the one that closely integrates flow solver and optimizer. For mildly nonlinear problems, the black-box approach may be sufficient. However, for highly nonlinear problems characterized by large Reynolds numbers, the black-box method is inefficient and may not even converge. Several measures can be taken to improve it.

First, a continuation scheme on Reynolds number may be adopted within the optimization. Suppose we want to optimize a fluid flow of a certain Reynolds number, *Re.* Instead of treating it as a single optimization problem, as is done in Algorithm 1, we decompose it into *m* optimization subproblems, corresponding to a sequence of increasing Reynolds numbers.

[2] **That is, the movement of the mesh due to a movement of the boundary is computed by treating the domain as an elastic medium; the fluid mesh may double as the solid mesh. The derivative of the domain mesh points with respect to the boundary mesh points is then easily obtained by differentiating the discrete solid equilibrium equations.**

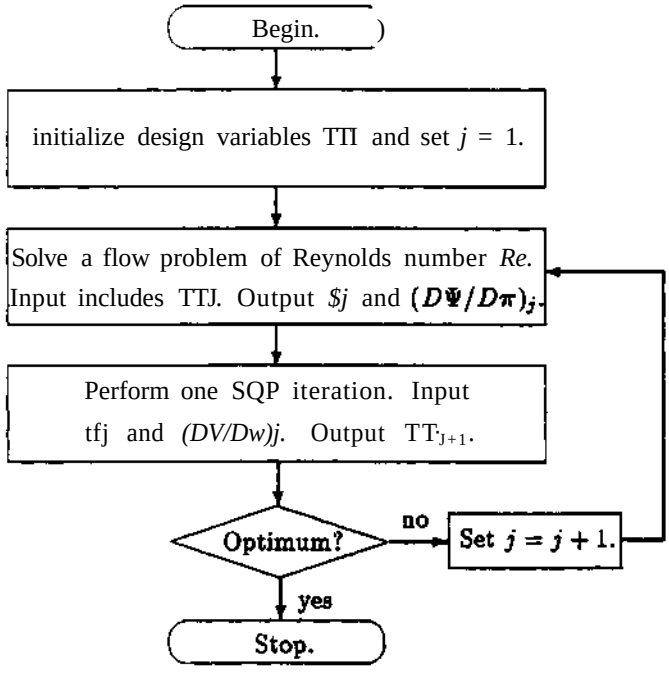

Figure 1: Algorithm 1.

For instance, if we let the Reynolds numbers increase by an equal increment *ARe = Re/m*, then the ith subproblem is to solve the optimization problem under a flow of Reynolds number *i ARe* $(1 \leq i \leq m)$. We use the optimum shape $TT^{\wedge"^{1}}$) of the (t - l)th subproblem as an initial guess for TT^ of the ith subproblem. This simple continuation on *Re* within optimization plays a role similar to the continuation, also on *Re,* in the solution of Navier-Stokes equations. Since this process generates better initial guesses for the NLP, it will tend to improve the chances of convergence, as well as the speed with which it will occur.

Second, we use the BFGS approximation of the Lagrangian Hessian matrix $H^{\wedge""^{1}}$ and Lagrange multipliers $A^{\wedge"^{1}}$ provided by the (i — l)th subproblem as starting points for H^ and A^, respectively, of the ith subproblem. Since our SQP algorithm builds a quasi-Newton approximation to the Lagrangian Hessian, and since the continuation scheme solves a sequence of related problems, it is reasonable to expect that $H^{\wedge""^{1}}$) possesses useful information for the i-th subproblem. A similar argument applies to the Lagrange multipliers. If we can provide good initial approximations not only to the shape parameters but also to the Hessian matrix and Lagrange multipliers, the number of optimization iterations should be significantly reduced.

Third, we establish good approximations for the state variables at each iteration beyond the first of each subproblem. A series of flow problems corresponding to a sequence of related shapes must be solved when the i-th subproblem is solved with SQP. From one shape to the next, the shape variables change from those of the previous shape by an amount ATT. The state variable shape Jacobian matrix *du/dir* has been computed at the previous shape, if we use the direct differentiation, as opposed to the adjoint, method. A first order approximation of the change in the state variables due to a change in the design variables can be found by multiplying the state variable shape Jacobian matrix by the design variable change vector.

Thus, for each new shape given by

$$\text{TTW} + \text{ATTW}, \tag{23}$$

we initiate the flow solution with

$$\mathbf{u}(\ 0+(\ |\ )^{1\ 0}\ \Delta\mathbf{\theta}\ , \tag{24}$$

where uW is the vector of converged state variables corresponding to the shape TTW. By introducing an improved approximation for the flowfield using existing sensitivity information, we reduce the number of required iterations significantly. This device has been proposed in [18] in the context of nonlinear elastic problems.

The continuation-SQP algorithm is summarized in Figure 2. Compared with Algorithm 1, Algorithm 2 more tightly couples the optimizer with the flow solver. Flow solution is carried out only to the Reynolds number associated with the current subproblem, and good initial approximations are generated for shape parameters, state variables, Lagrange multipliers, and the Hessian matrix, using available information. We expect a significant improvement in performance, especially for highly nonlinear problems.

5. **Optimal Design of** a **2D Tube**

We consider a two dimensional tube, shown in Figure 3a, with a corresponding mesh in Figure 3b, in which fluid enters horizontally from the left, undergoes a 90° bend, and exits downward in the vertical direction. This is a simplified model for a blood flow cannula of an artificial heart device. It is assumed that the tube has a uniform section with a width or diameter *d.* The problem is to design the shape of the middle axis of the tube, such that a combination of the objective functions in Equations (7)-(9) is minimized subject to certain geometric constraints. In this paper, the examples solved do not include the flow constraints requiring that the local functions (4)-(6) not exceed certain allowable values everywhere in the flow domain. The shape of the middle axis is a function *r(9)* in the polar coordinate system, and it can be represented by a cosine series

$$r(9) = \sum_{i=0}^{p-i} Y,\ ricos(2i0),\quad 9\ 6\ [0°,90°]. \tag{25}$$

The coefficients r_{2-}, $i = 0, \ldots, P - 1$ are thus our design variables.

The middle axis *r(9)* is subject to one of the following end constraints:

- both positions of entrance and exit are fixed, specifically, r(90°) = 71 and r(0°) = 72;
- the entrance is fixed while the exit position is allowed to vary within a given range, i.e., r(90°) = 71 and $7^{\wedge} \leq$ r(0°) $\leq$ 7?;
- the entrance position is allowed to vary within a given range while the exit is fixed, i.e., $-y[\_\leq$ r(90°) $\_\leq$ 7? and r(0°) = 72;
- both positions of entrance and exit are allowed to vary within given ranges, namely, $7\dot{1} \leq$ **r(90°)** $\leq$ 7? and $72 \leq$ *r(0°)* $\leq$ 7?-

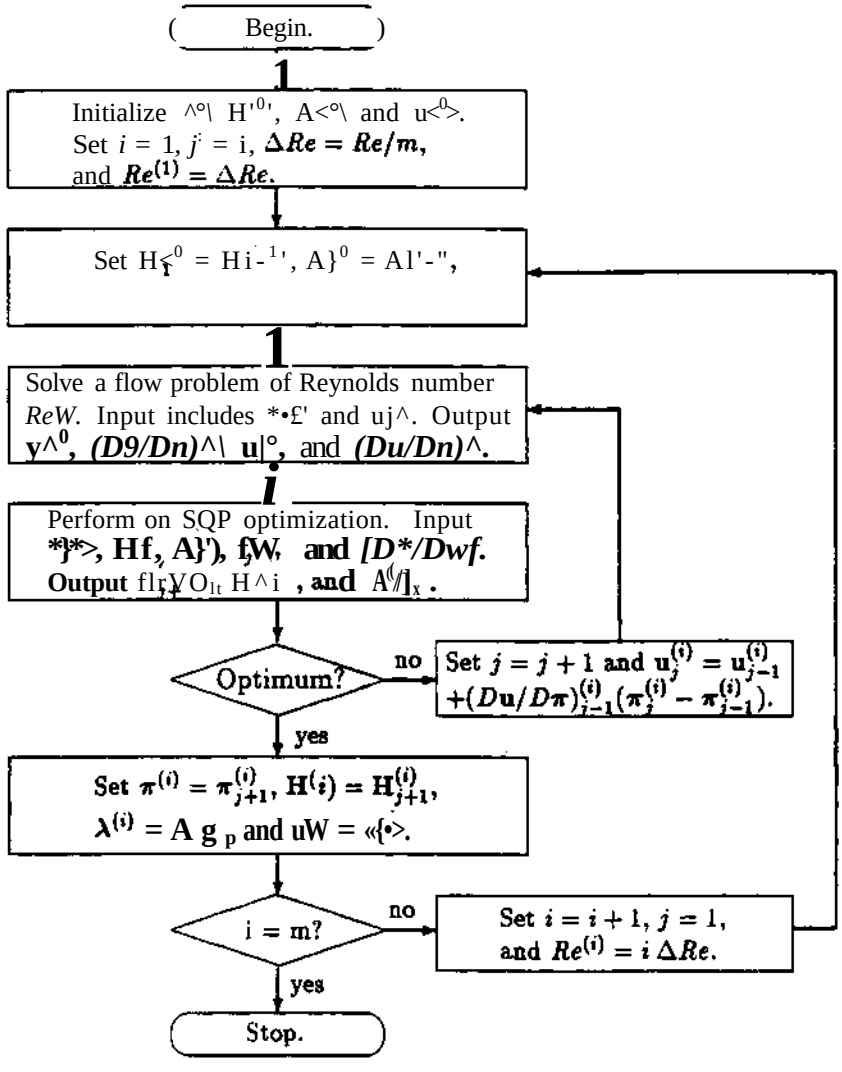

Figure 2: Algorithm 2.

These conditions impose linear constraints on the design variables, since

$$r(0°) = \sum_{i=0}^{1} r_i, \qquad r(90°) = \sum_{i=0}^{1} (-1)^i r_i. \tag{26}$$

In addition, design variables have to satisfy certain conditions to ensure a valid shape; otherwise, invalid shapes such as the one shown in Figure 3c may arise (as it actually did). Since we deal only with a discretized geometric model of the tube, shape constraints need only be imposed at K distinct points $(r(0_t),0_t)$, $i = 1,\ldots,K$, uniformly spaced along the middle axis of the tube. First, $r(0)$ must be non-negative:

$$r(0_t) \geq 0, \quad i = 1,\ldots,K \tag{27}$$

Second, the shape cannot penetrate into itself:

$$(\bar{x} - x_{0,i})^2 + (\bar{y} - y_{0,i})^2 \geq d^2 \tag{28}$$

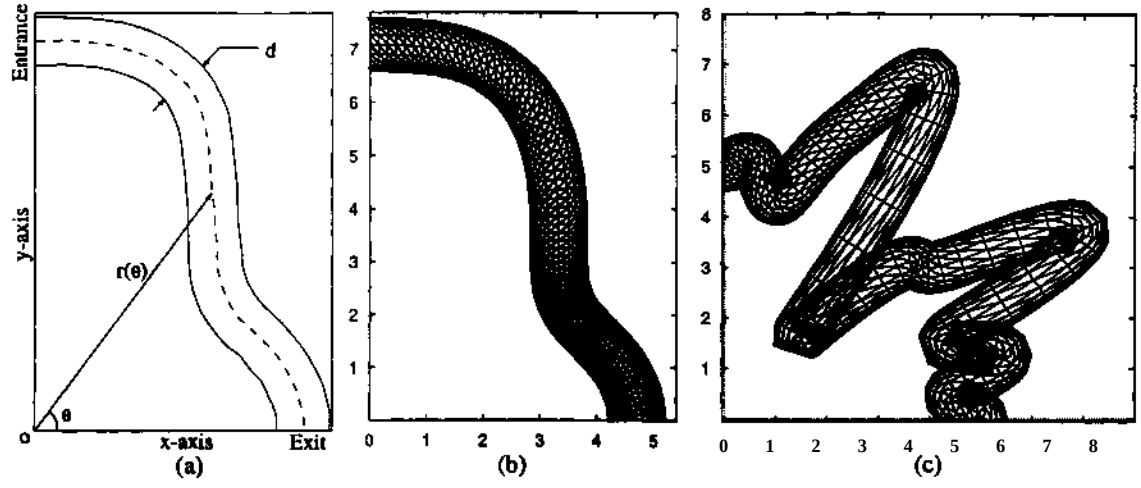

Figure 3: 2D tube: (a) geometry, (b) computational mesh, (c) invalid shape.

$$(\bar{x} - x_{0,i+1})^2 + (\bar{y} - y_{o,i+i})^2 \geq \frac{1}{4}d^2 \qquad i = 1, \ldots, K. \tag{29}$$

Here, (xo,i, ,t/o;t) is the Cartesian coordinate of the ż-th node along the middle axis of the tube; $(\bar{x}, \bar{y})$ is the coordinate of the intersection point of the two lines perpendicular to each other and passing through ($x_{o,t'}$ 2/o;t) and (xo,;+i, 2/o;t+i)- The values of ($\bar{x}$,$\bar{y}$) and (xo,t, 2/o,t) are computed with the following formulae:

$$\bar{x} = A_r/A\,, \qquad \bar{y} = A_y/A \tag{30}$$

$$\Delta_x = l_{y,i}l_{y,i+1}(y_{oj} - 3/0{,}1{+}1) + z0,_i l_{x,i}l_{y,i+1} - x_{0,i+1}l_{y,i}l_{x,i+1} \tag{31}$$

$$\Delta_y = l_{x,i}l_{x,i+1}(x_{0,i+1} - x_{0,i}) + y_{0,i+1}l_{x,i}l_{y,i+1} - y_{0,i}l_{y,i}l_{x,i+1} \tag{32}$$

$$\Delta = l_{x,i}l_{y,i+1} - l_{y,i}l_{x,i+1} \tag{33}$$

$$x_{:0(}- = r(0i)\cos 0\{\,, \qquad ?/o,t = r(\theta_i)\sin\theta_i \tag{34}$$

$$l^{r} - \frac{r'(0i)\cos 0i - r(0i)\sin 0i}{[(dr(9i)/d0)^* + r(0i)^*]^{1/2}} \tag{35}$$

$$l_{y,i} = \frac{r'(\theta_i)\sin\theta_i + r(\theta_i)\cos\theta_i}{[(\partial r(\theta_i)/\partial\theta)^2 + r(\theta_i)^2]^{1/2}} \tag{36}$$

$$r'(\theta_i) = \frac{\partial r(\theta_i)}{\partial\theta}\,. \tag{37}$$

We have developed a code that couples optimization and flow solution based on Algorithms 1 and 2 of Section 4. The flow solver employs triangular Taylor-Hood elements, i.e., a piecewise quadratic approximation of the velocity field and a piecewise linear approximation of the pressure field are made. The Taylor-Hood element is known to be stable in the sense of Babuska-Brezzi, and produces errors of order h^3 for velocity and h^2 for pressure [9]. A banded *LU* factorization routine from the LAPACK library [6] is used to solve the linear systems that arise at each step of Newton's method. Analytical gradients of the objective functions are computed using the direct sensitivity analysis method indicated in Equation 22 and the formulae derived in [10], while the gradients of the constraints can be obtained from Equations (26)-(37).

6. Numerical Results

In this section we present some representative numerical results. Specifically, we compare the performance of Algorithms 1 and 2 of Section 4, as well as the influence of the initial shape, number of design variables, end constraints on the tube, Reynolds number, and choice of objective function, on the resulting optimal shape. Unless otherwise stated, the following data apply to all cases: the Reynolds number, estimated based on the average flow velocity at the entrance and a tube diameter of d = 1, is 1000; both entrance and exit are fixed at r = 5.1; the objective function is the integral of the dissipation function ¶; the number of design variables, i.e. the number of terms in the series (25), is taken to be 14; and the termination criterion is that the Euclidean norm of the projected gradient (i.e. the Kuhn-Tucker optimality condition, KTO) is less than 5×10^{-9}. The computations are performed on a Digital 3000-400 (Alpha) workstation equipped with 128Mb of memory.

Table 1 compares the performance of Algorithms 1 and 2 of Section 4, along with an algorithm named 2- that is intermediate between the two. Algorithm 2- improves on Algorithm 1 by extending continuation on Reynolds number to the optimization level, as in Algorithm 2, but does not include any of the other features. The table compares the total number of optimization iterations, the total number of *LU* factorizations of the Jacobian of the state equations with respect to the state variables, CPU time, and total elapsed time. The cost of a single flow solution at the optimum is also included for comparative purposes. The number of *LU* factorizations is a good measure of state variable-scalability, since for high Reynolds numbers, flow solution and hence *LU* factorization will dominate the other computations (computing the objective and constraint gradients, finding a basis for the null space of the constraints, performing the quasi-Newton updates, and solving the reduced Hessian system). Both algorithms were initiated from the same shape, which is depicted in Figure 5a.

Table 1; Algorithm comparison.

Comparison Items	Optm iter	*LU* fact	CPU (in clock ticks)	Elapsed time (in seconds)
Algorithm 1	46	6,455	3,335,313	61,054
Algorithm 2-	68	2,622	1,595,781	29,534
Algorithm 2	50	1,350	866,870	15,067
1 flow soln	—	100	55,058	923

Algorithm 2 is seen to be about half an order of magnitude more efficient than Algorithm 1. This is due to the continuation features described in Section 4. Furthermore, we see that the total cost of solving the optimization problem is about 16 times more expensive than performing a flow simulation, a factor about equal to the number of design variables (which is 14). We remark that a *direct search method,* i.e. a method that does not exploit derivative/curvature information and instead relies on some form of explicit or implicit "enumeration" of the design space, cannot possibly be competitive with an SQP-based method for this class of problem. The reason is that 16 samples of 14-dimensional space are unlikely to yield any useful information for such methods, which typically require a large number (relative to the dimension of the space) of function evaluations to identify the region surrounding a minimizer.

Table 2 shows the numbers of optimization iterations and *LU* factorizations taken by the two continuation algorithms for successive values of *Re.* The results show the improved

convergence due to initiating the Hessian matrix and Lagrange multipliers with values from the previous Reynolds number problem, i.e. reductions from 15 to 7, 16 to 11, and 16 to 11 in the number of optimization iterations for second, third, and fourth subproblems, respectively. Furthermore, Table 2 shows the effect of using sensitivity information to improve the initial guess of the flowfield, namely Equation 24. The resulting reduction in number of *LU* factorizations is significant.

Table 2: Breakdown of optimization iterations and *LU* factorizations for successive *Re*.

Re	Algorithm 2-		**Algorithm** 2	
	Optm iter	*LU* fact	**Optm** iter	*LU* fact
250	21	131	21	119
500	15	667	7	98
750	16	836	11	574
1000	16	988	11	559

Table 3 shows the effect of initial shape on the optimum. The optimizer is initiated with two quite different shapes. The shape of Case I is depicted in Figure 4a, while that of Case II is shown in Figure 5a. Table 3 lists initial and optimum values of the design variables, objective function, and optimality condition. Clearly both initial shapes are far from optimum as well as from each other, as evidenced visually and by the values of their optimality condition. However the optimal dissipation agrees to eight digits, and the optimal values of the design variables agree to four. The optimal shapes shown in Figure 4b and Figure 5b for Case I

Table 3: Effects of initial shapes on optimum.

Items	Case I		Case II	
	Initial	Optimum	Initial	Optimum
r_1	5.4000	5.1065820	5.6109985	5.1065841
r_2	-1.500	0.0837369	0.0000000	0.0837377
r_3	0.6000	0.0249086	-0.7800000	0.0249068
r_4	0.3000	-0.0337325	0.0000000	-0.0337311
r_5	-0.1000	-0.0094676	0.2400000	-0.0094694
r_6	0.0100	-0.0171818	0.0000000	-0.0171821
r_7	-0.0050	-0.0069715	-0.1100000	-0.0069711
r_8	0.0000	-0.0107487	0.0000000	-0.0107495
r_9	0.0000	-0.0051330	0.0600000	-0.0051324
r_{10}	0.0000	-0.0080299	0.0000000	-0.0080313
r_{11}	0.0000	-0.0047271	-0.0300000	-0.0047273
r_{12}	0.0000	-0.0073294	0.0000000	-0.0073294
r_{13}	0.0000	-0.0051915	0.0200000	-0.0051907
r_{14}	0.0000	-0.0067146	0.0000000	-0.0067144
$\bar{\Phi}$	43.889	10.958633	33.321813	10.958633
KTO	1.668D+5	1.649D-9	5.181D-I-4	4.002D-9

and Case II, respectively, are indistinguishable from each other. Although it is unlikely that convexity of the optimization problem can be proven, we have always obtained the same optimal shape regardless of the starting shape, for our particular choice of shape variables. Similar results are observed for other choices of objectives function, suggesting uniqueness of the minimum obtained.

Figure 4 demonstrates the dependence of the optimum shape on the number of design variables chosen. Figure 4b shows the 14-variable optimal shape and corresponding stream-

lines. Figure 4c depicts the optimal shape and its streamlines found with 7 design variables. The objective function values for optimum shapes with 14 and 7 design variables are, respectively, 10.96 and 11.21. We see that the optimum shapes obtained with 14 and 7 design variables are not substantially different. This suggests an additional improvement in efficiency that can be realized when hierarchical families of design variables are used. Namely, one may solve a shape optimization problem with a small number of shape variables, increase the number of design variables, re-solve the optimization problem initiated by the smaller problem's Lagrange multipliers, Hessian approximation, and design variables, and repeat.

Figure 5 illustrates the influence of the end constraints on the optimal shape and streamlines. The two sets of end constraints considered are: 1) both entrance and exit are fixed at r = 5.1; 2) the entrance is allowed to vary within a range 4.0 $\leq$ r(90°) $\leq$ 7.0 while exit is fixed at r(0°) = 5.1. We see that by freeing the position of the entrance, the optimum favors a tighter radius at the inflow. This can be explained as follows. The objective function is an integral (of the dissipation function) over the flow domain. Both greater values of dissipation as well as larger domain areas serve to increase this function. By reducing the radius at the entrance, the area and thus objective function are reduced, all else being equal. Reducing the radius, however, increases the dissipation, for the flow must change direction over a smaller distance. Thus, the optimum entrance radius does not assume its lower bound, and the optimizer strikes the best balance between these conflicting goals. The optimum objective function value for the free-fixed case is expected to be smaller than that of the fixed-fixed case, because the former is less constrained than the latter. We obtain exactly this result, with an optimum ¥ of 10.72 (free-fixed) and 10.96 (fixed-fixed).

Figure 6 compares the optimal shapes obtained under Reynolds numbers of 100, 300, and 1000. Here, the integral of the magnitude of vorticity $\overline{u}$ is the objective function. The entrance is allowed to vary within a range 4.0 $\leq$ r(90°) $\leq$ 7.0, and the exit is fixed at r(0°) = 5.1. The figure shows that for Re = 100, the optimum shape is characterized by a relatively straight region in the interior connected to sharply curving entrance and exit segments. This is a manifestation of the behavior observed in the previous paragraph. The optimizer biases the design towards one with smaller area. The smallest area is achieved by a straight line between entrance and exit. The rapid change in entrance and exit curvature of the tube necessary to realize this is deleterious for the objective. Therefore, the ends are rounded to smooth the flow passage. However, as the Reynolds number increases, the additional vorticity induced by the rounded ends more than offsets the decrease in area achieved by the straight segment. The optimizer thus increases the curvature of the middle segment and decreases that of the ends. This is observed for Re=300 and 1000. Optimal values of the objective $\overline{\$}$ increase with Re as expected; the corresponding optima for Reynolds numbers of 100, 300, and 1000 are 0.09533, 0.8867, and 10.96, respectively.

Figure 7 shows the effect of choice of objective function on the optimal shape. The entrance is allowed to vary within a range 4 $\leq$ r(90°) $\leq$ 7, and the exit is fixed at r(0°) = 5.1. The group of functions $\overline{4}$, $\overline{r}$ and $\check{c}J$ tends to give one set of optimal shapes similar to each other, while the other group of objectives $\hat{\$}$, f and $\hat{u}$ leads to another set of optimum shapes, also similar to each other but quite different from the first group. Again, the first group of objectives invokes the optimizer's preference for smaller areas; thus, the tightening of the entrance radius of curvature Figures 7a-c. On the other hand, the second group's objectives functions are scaled by the area of the domain; thus, the optimizer is free to concentrate on minimizing the objective at hand (dissipation, vorticity, or shear stress) without area

penalty. Figures 7d-f show the result: a larger radius of curvature at the exit.

7. Conclusions And Future Work

We have considered the problem of shape optimization of systems governed by the incompressible Navier-Stokes equations. In particular, we have considered objective functions motivated by design of artificial heart components. These functions are directly and indirectly related to blood damage, and include the rate of mechanical energy dissipation due to viscosity, the magnitude of vorticity, and the maximum shear stress.

We have introduced a continuation-SQP algorithm that promotes the Reynolds number continuation strategy of the solver to the optimizer. In addition to the design variables, simple continuation is conducted on the quasi-Newton approximation of the Hessian matrix of the Lagrangian function, as well as on the Lagrange multipliers. Numerical experiments have been conducted on a problem of finding the optimal shape of a blood transport conduit. The results indicate that this algorithm reduces by a factor of four the time consumed by a standard **SQP** algorithm, which is already an efficient method relative to gradient-only or direct search methods.

At present, our algorithm has been applied to two-dimensional problems possessing simple geometry. Work is underway to extend its applicability to complex three-dimensional geometries, including a full ventricular assist artificial heart device. The major challenges for such problems are those related to geometry (how to automatically parameterize complex shapes, how to ensure shape validity), to the large-scale nature of the problem, and to the incorporation of non-Newtonian constitutive laws to better describe blood flow, as well as more precise blood damage models to be used as objective functions. At present, the geometric issues have been addressed in an *ad hoc* fashion, i.e. tailored to the specific geometry at hand (our continuation-SQP algorithm on the other hand is completely general). A promising approach to automate the geometric aspects of shape optimization for arbitrary geometries is the skeletal method of [17]. With regard to the difficulties induced by the large number of design and state variables inherent in three dimensions, a framework for addressing these problems is contained within the parallel reduced SQP method of [14]. We intend to incorporate aspects of these approaches into our continuation-SQP algorithm.

Though our work has been limited to two dimensions, our results indicate that improvements in optimization algorithms and computing power make it feasible to find optimal shapes of systems governed by incompressible Navier-Stokes equations in several hours on a desktop workstation, for simple geometries and flow regimes of interest in biomechanics. With the aid of parallel supercomputers, we anticipate optimizing complex three-dimensional flows of medical interest in the near future.

References

[1] G.W. Burgreen and O. Baysal. Three-dimensional aerodynamic shape optimization of wings using sensitivity analysis. AIAA Paper 94-0094.

[2] H. Cabuk, C.H. Sung, and V. Modi. Adjoint operator approach to shape design for

internal incompressible flows. In G.S. Dulikravich, editor, *Third International Conference on Inverse Design and Optimization in Engineering Sciences*, pages 391-404, Washington D.C., October 1991.

[3] I-C. Chang, F.J. Torres, and C.P. van Dam. Wing design code using three-dimensional Euler equations and optimization. AIAA Paper 91-3190.

[4] G.B. Cosentino and T.L. Hoist. Numerical optimization design of advanced transonic wing configurations. *Journal of Aircraft*, 23(3):192-199,1986.

[5] M.E. Eleshaky and 0. Baysal. Airfoil shape optimization using sensitivity analysis on viscous flow equations. *ASME Journal of Fluids Engineering*, 115(3):75-85,1993.

[6] E. Anderson et al. *LAPACK Users' Guide*. SIAM, Philadelphia, 1992.

[7] R. Fletcher. *Practical Methods of Optimization*. Wiley-Interscience, 1987.

[8] R. Glowinski and 0. Pironneau. On the numerical computation of the minimum drag profile in laminar flow. *Journal of Fluid Mechanics*, 72:385-389,1975.

[9] M. Gunzburger. *Finite Element Methods for Viscous Incompressible Flows*. Academic Press, 1989.

[10] B. He and 0. Ghattas. Discrete sensitivity analysis of Navier Stokes equations, working manuscript.

[11] R. Hicks and P.A. Henne. Wing design by numerical optimization. In *Proceedings of the AIAA Aircraft Systems and Technology Meeting*, 1977.

[12] W. Hock and K. Schittkowski. A comparative performance evaluation of 27 nonlinear programming codes. *Computing*, 30:335-358,1983.

[13] M.E. Lores, P.R. Smith, and R.M. Hicks. Supercritical wing design using numerical optimization and comparisons with experiment. AIAA Paper 79-0065.

[14] C.E. Orozco and O. Ghattas. Massively parallel aerodynamic shape optimization. *Computing Systems in Engineering*, 1-4:311-320,1992.

[15] O. Pironneau. On optimum design in fluid mechanics. *Journal of Fluid Mechanics*, 64(l):97-110, 1974.

[16] J. Reuther, S.E. Cliff, R.M. Hicks, and C.P. van Dam. Practical design optimization of wing/body configurations using euler equations. *AIAA Paper*, 92-2633.

[17] G. Turkiyyah and 0. Ghattas. Geometric reasoning for shape design. In *Proceedings of the Ninth AAAI Conference*. AAAI Press, 1991.

[18] C.C. Wu and J.S. Arora. Simultaneous analysis and design of nonlinear response. *Engineering with Computers*, 2(l):53-63, 1987.

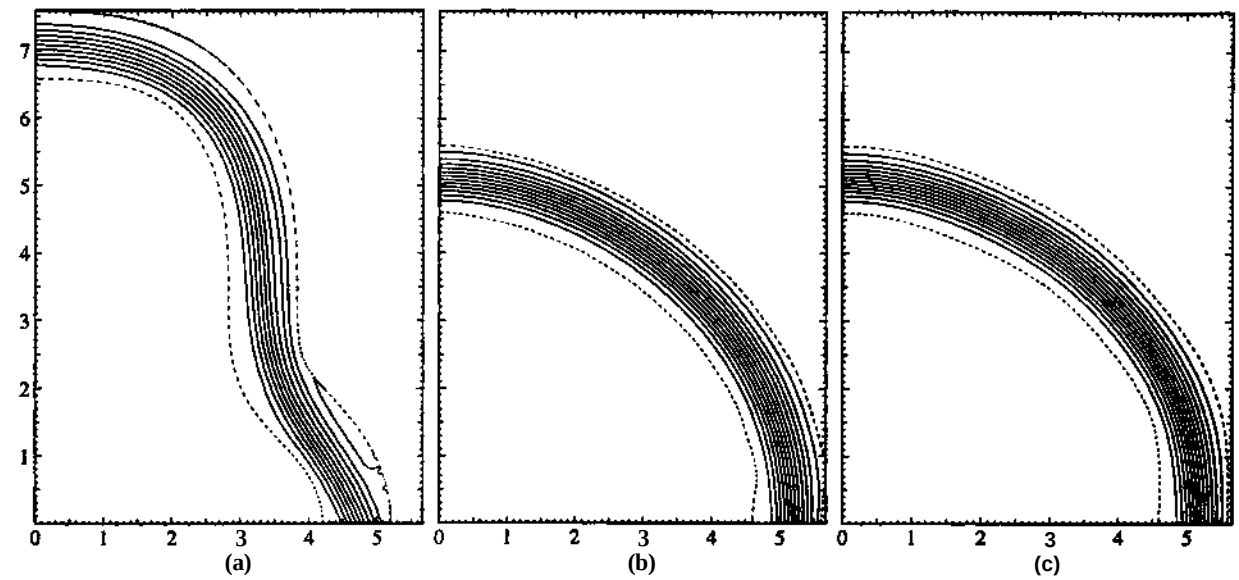

Figure 4: Initial and optimum shapes: (a) Initial, (b) optimum with 14 design variables, (c) optimum with 7 **design variables.**

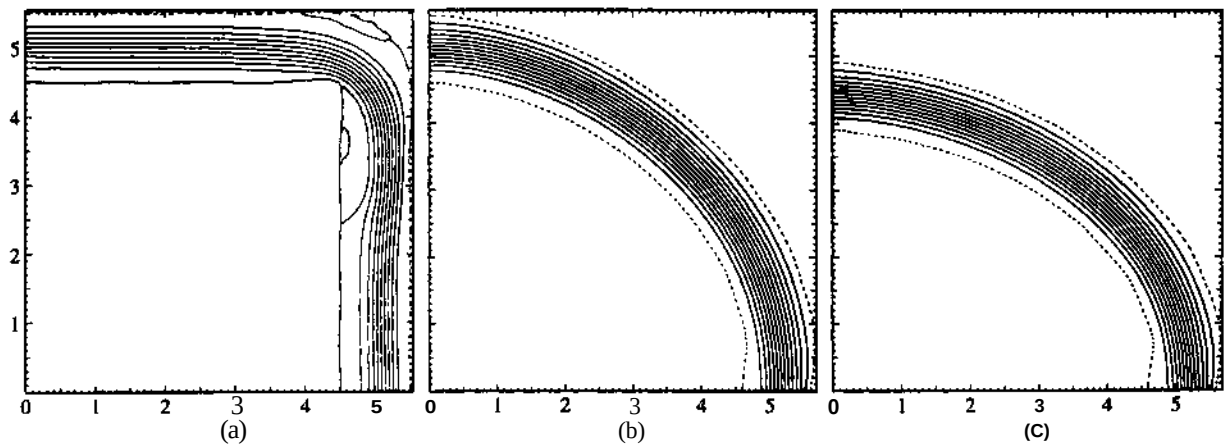

Figure 5: Initial and optimum shapes: (a) Initial, (b) optimum with entrance and exit fixed at r = 5.1, (c) optimum with entrance 4 < **r(0°)** < 5 and exit r(90°) = 5.1.

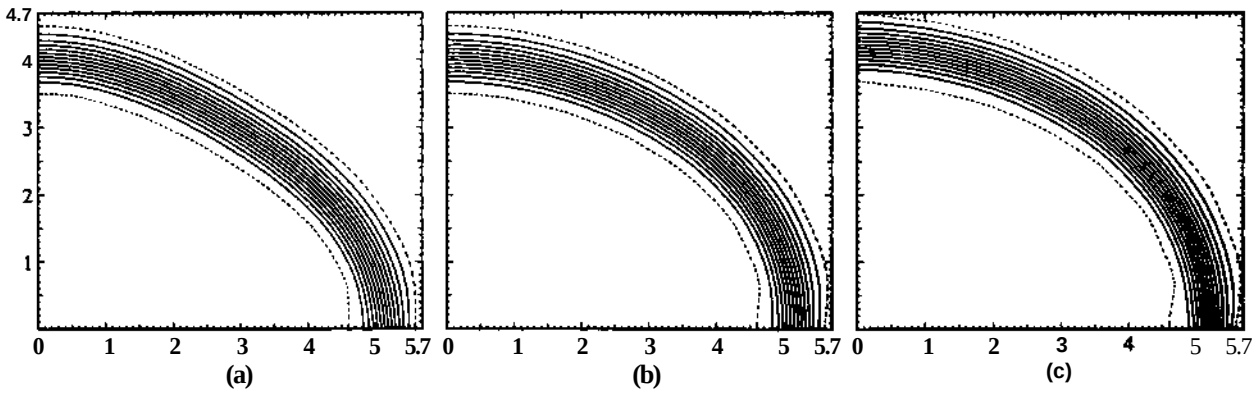

Figure 6: Optimal shapes **for different Re: (a) 100, (b) 300, (c) 1000.**

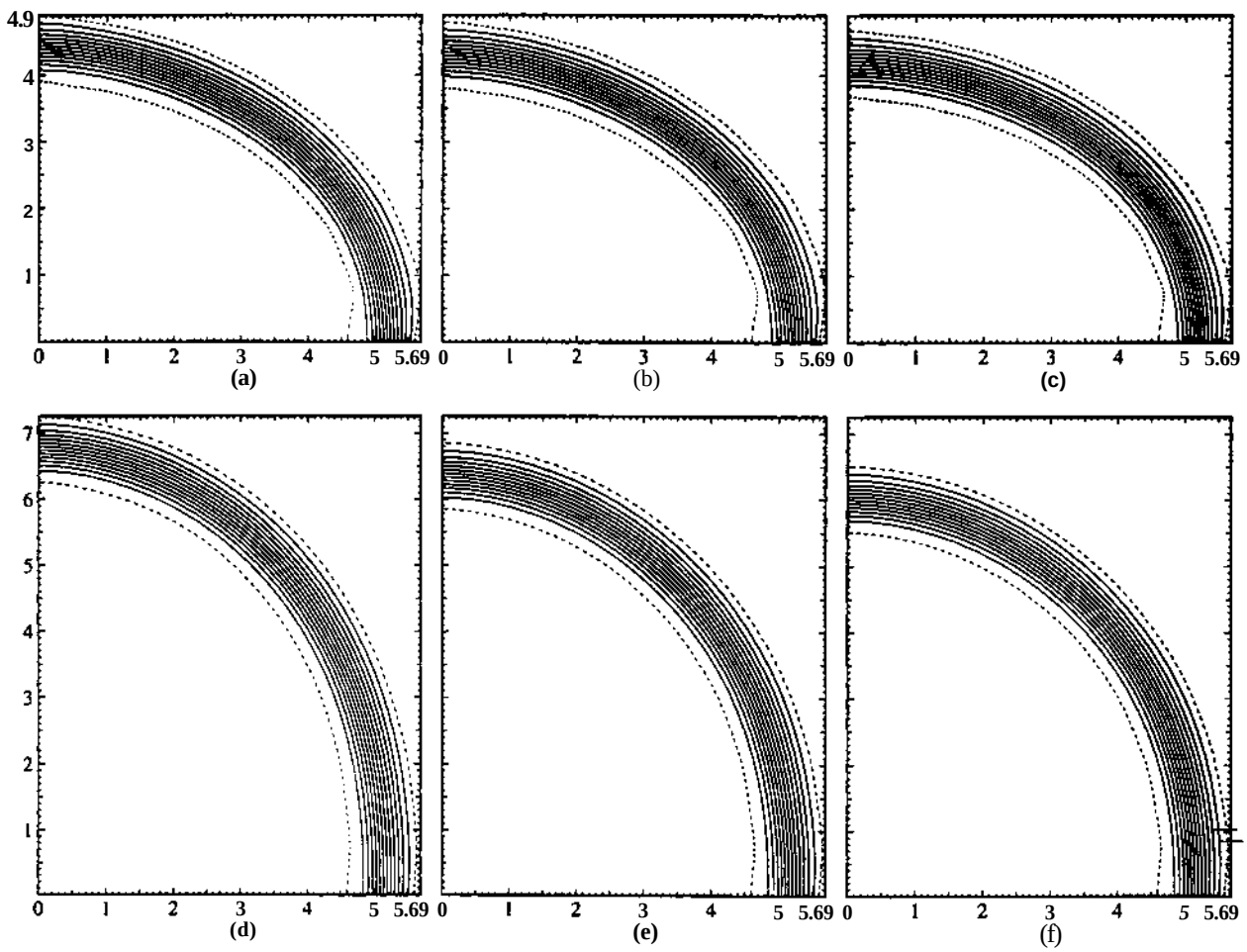

Figure 7: Optimum shapes for different objective functions: (a) $\overline{\$}$, (b) $\overline{r}$, (c) $\overline{57}$, (d) $\hat{\$}$, (e) $\hat{r}$, (f) Q.